

Title	The effect of model inaccuracy and move-blocking on the performance of a wave-to-wire wave energy converter , under economic predictive control
Authors	O'Sullivan, Adrian C. M.;Lightbody, Gordon
Publication date	2017-08-30
Original Citation	O'Sullivan A. C. M. and Lightbody G. (2017) 'The Effect of Model Inaccuracy and Move-blocking on the Performance of a Wave-to-wire Wave Energy Converter, under Economic Predictive Control', 12th European Wave and Tidal Energy Conference (EWTEC), Cork, Ireland, 27 August - 1 September.
Type of publication	Article (peer-reviewed)
Link to publisher's version	<a href="http://www.ewtec.org/proceedings/">http://www.ewtec.org/proceedings/</a>
Rights	© 2017 EWTEC
Download date	2025-04-18 04:03:04
Item downloaded from	<a href="https://hdl.handle.net/10468/4702">https://hdl.handle.net/10468/4702</a>



# UCC

**University College Cork, Ireland**  
Coláiste na hOllscoile Corcaigh

# The Effect of Model Inaccuracy and Move-blocking on the Performance of a Wave-to-wire Wave Energy Converter, under Economic Predictive Control

Adrian C.M. O’Sullivan<sup>a,b</sup>, Gordon Lightbody<sup>a,c</sup>

<sup>a</sup>Department of Electrical and Electronic Engineering University College Cork, Ireland

SFI Research Centre for Marine and Renewable Energy, MaREI

<sup>b</sup>adrian.osullivan@umail.ucc.ie, <sup>c</sup>g.lightbody@ucc.ie

**Abstract**—In this paper, an economic Model Predictive Control (MPC) is used to investigate the effects that arise from the model mismatch between the control and the system. It is shown that the average electrical power is affected by the modelling discrepancies, but that the performance is still acceptable. A move-blocking technique is incorporated into the structure of the control horizon of the MPC, where the move-blocking decreases the computational burden whilst maintaining system performance, hence drastically reducing the optimisation solving time. The MPC with the move-blocking incorporated is then tested on the most significant mismatch, where it is shown that the control horizon of the MPC can be drastically reduced while maintaining system performance.

**Index Terms**—Model predictive control; Electrical optimisation; System mismatch; System Robustness

## I. INTRODUCTION

Many wave energy converter (WEC) designs have been proposed to maximise the power extraction from ocean waves, [1]. In the work presented here a cylindrical point absorber with a semi-hemispherical base is used due to its simplistic linear design and suitability for array formations [2]. A linear permanent magnet generator (LPMG) is utilised as a realistic power take off (PTO) to produce the control forces leading to power maximisation.

In recent times the importance of active control for WEC systems has been emphasised, as it allows for greater power extraction while protecting the device. One of the first control techniques to be used was reactive control (impedance matching) [3], in which the velocity of the WEC is controlled to be in phase with the monochromatic excitation force. This effectively produces impedance matching which results in maximum average power. Latching control is another type of classical control that was developed for monochromatic waves [4]. Latching control produces a similar phase lock effect to the reactive control, except that it uses a discontinuous control force to control the system. These methods were originally developed for monochromatic excitation waves, though some have been adapted to accommodate polychromatic irregular excitation waves, with suboptimal performance [5], [6].

Lately there have been further developments in advanced control methods, such as bang-bang [7], pseudo spectral [8]

and MPC [9]. In this work, MPC is utilised because of its ability to produce optimal results in the presence of realistic mechanical and electrical constraints. MPC maximises the average power over a prediction horizon by minimising an economic cost function [10]. It has been shown in [11], that simply maximising the mechanical average power was insufficient when extracting electrical power; therefore including the PTO losses within the optimisation was shown to be imperative.

In previous work [12], a long prediction horizon and a perfect (matched) model was assumed, hence allowing the control system to produce the ideal optimal control for the system. In this work the effects of model mismatch and optimisation simplification is examined. Since WEC dynamics can be uncertain and may indeed vary over their lifetime, due for example to biofouling [13], the performance of the control system may therefore in reality become sub-optimal, leading to mechanical and electrical degradation if the systems constraints are exceeded. Here a study is presented to investigate how the performance of a point absorber under MPC depends on the model accuracy.

Constrained optimisation forms the basis of most MPC control laws, which makes it advantageous over other control methods. However, the computational load that comes with it is undesirable [14]. In this work, an assessment of different control horizon curtailments is carried out to try to simplify the online complexity of the MPC optimisation, whilst not sacrificing the performance of the system. Using a move-blocking technique [15], the number of free variables in the control horizon can be drastically reduced while maintaining a similar high performance as a standard economic MPC with a longer control horizon. This curtailment reduces the amount of unnecessary computational power that would have previously been used to calculate the inconsequential control horizon variables.

The performance of the MPC with reduced control horizon is then analysed when a model mismatch occurs between the control and system. This shows that there needs to be a balance where the minimum control horizon is found while maintaining high performance.

## II. MODELLING

### A. Hydrodynamics

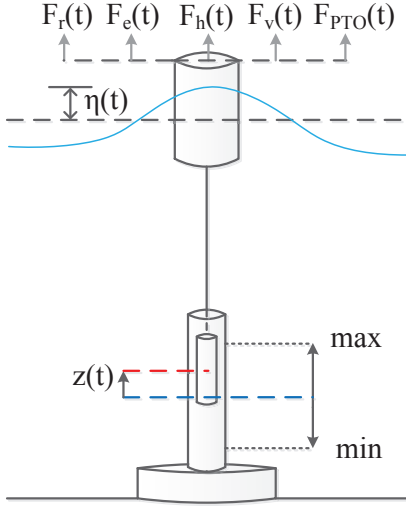


Fig. 1. System model with WEC and PTO

A cylindrical wave energy converter point absorber which is restricted to move in the heave direction is assumed in this paper. The model is based on linear wave theory. The hydrodynamic model (1), as shown in Fig. 1, consists of the hydrostatic force  $F_h(t)$ , the radiation force  $F_r(t)$ , the excitation force  $F_e(t)$ , controlled PTO force  $F_{PTO}(t)$  and the non-linear viscous force  $F_v(t)$ . Initially in this paper,  $F_v(t)$  is neglected, since it adds unnecessary complexity into the individual characteristic mismatch analysis.

$$M\ddot{z}(t) = F_h(t) + F_r(t) + F_e(t) + F_v(t) + F_{PTO}(t) \quad (1)$$

This could be modelled as the integro-differential equation (2), where the WEC heave displacement is  $z(t)$ , WEC velocity is  $\dot{z}(t)$ , the wave elevation is  $\eta(t)$  and the wave velocity  $\dot{\eta}(t)$ . The hydrostatic force  $F_h(t)$  is a function of the displacement  $z(t)$ , where  $\beta$  is the linear hydrostatic spring constant. The radiation force  $F_r(t)$  is a convolution integral from the Cummins transformation [16], where the radiation kernel  $h_r(t)$  and the added mass  $m_\mu$  are found using WAMIT [17]. The non-linear viscous force  $F_v(t)$  depends on the relative velocity between the WEC and wave and the PTO force  $F_{PTO}(t)$  is a control system produced force,

$$(M + m_\mu)\ddot{z}(t) + \int_0^t h_r(\tau)\dot{z}(t - \tau)d\tau + \beta z(t) + C_{vis}(t)(\dot{z}(t) - \dot{\eta}(t)) = (M + m_\mu)(u_q(t) + v(t)) \quad (2)$$

where the scaled forces,  $u_q(t)$  and  $v(t)$  are,

$$u_q(t) = \frac{F_{PTO}(t)}{M + m_\mu} \quad v(t) = \frac{F_e(t)}{M + m_\mu} \quad (3)$$

The excitation force  $F_e(t)$  is a non-causal convolution integral of the wave elevation  $\eta(t)$ , where the excitation kernel  $h_e(t)$  was found using WAMIT [17].

$$F_e(t) = \int_{-\infty}^t h_e(\tau)\eta(t - \tau)d\tau \quad (4)$$

The radiation kernel  $h_r(t)$  can be expressed as a summation of complex exponentials (5), where the parameters  $\mu_i$  and  $c_i$  can be found from impulse response data  $h_r(t)$  using Prony's method,

$$h_r(t) \approx \tilde{h}_r(t) = c_1 e^{\mu_1 t} + c_2 e^{\mu_2 t} + c_3 e^{\mu_3 t} + \dots + c_n e^{\mu_n t} \quad (5)$$

The radiation force,  $F_r(t)$ , can then be transformed into the Laplace domain as  $F_r(s) = sH_r(s)Z(s)$ , where,

$$H_r(s) = \mathcal{L}\{\tilde{h}_r(t)\} = \frac{b_m s^m + b_{m-1} s^{m-1} + \dots + b_0}{s^n + a_{n-1} s^{n-1} + \dots + a_0} \quad (6)$$

This is readily transformed into the following continuous time state-space model (7),

$$\begin{aligned} \dot{\mathbf{x}}_r(t) &= A_r \mathbf{x}_r(t) + B_r \dot{z}(t) \\ F_r(t) &= C_r \mathbf{x}_r(t) + D_r \dot{z}(t), \end{aligned} \quad (7)$$

where  $\mathbf{x}_r(t) \in \mathbb{R}^n$ ,  $A_r \in \mathbb{R}^{n \times n}$ ,  $B_r \in \mathbb{R}^n$ ,  $C_r \in \mathbb{R}^{1 \times n}$ .

By temporarily neglecting viscous effects, the entire continuous system can be represented in the following state-space format (8),

$$\frac{d}{dt} \begin{bmatrix} z(t) \\ \dot{z}(t) \\ \mathbf{x}_r(t) \end{bmatrix} = A_c \begin{bmatrix} z(t) \\ \dot{z}(t) \\ \mathbf{x}_r(t) \end{bmatrix} + B_c u_q(t) + F_c v(t) \quad (8)$$

$$A_c = \begin{bmatrix} 0 & 1 & \mathbf{0} \\ -\frac{\beta}{M+m_\mu} & -\frac{D_r}{M+m_\mu} & -\frac{C_r}{M+m_\mu} \\ 0 & B_r & A_r \end{bmatrix}$$

$$\mathbf{x}(t) = \begin{bmatrix} z(t) \\ \dot{z}(t) \\ \mathbf{x}_r(t) \end{bmatrix} \quad \mathbf{y}(t) = \begin{bmatrix} z(t) \\ \dot{z}(t) \end{bmatrix} \quad B_c = \begin{bmatrix} 0 \\ 1 \\ 0 \end{bmatrix},$$

where  $A_c \in \mathbb{R}^{(n+2) \times (n+2)}$ ,  $B_c \in \mathbb{R}^{(n+2) \times 1}$ ,  $F_c = B_c$ ,  $\mathbf{x}(t) \in \mathbb{R}^{(n+2) \times 1}$  and  $\mathbf{y}(t) \in \mathbb{R}^{2 \times 1}$

### B. Linear Permanent Magnet Generator PTO

In this paper, a realistic Power Take Off (PTO) utilising a converter connected Linear Permanent Magnet Generator (LPMG) is used to transfer electrical energy into a mechanical force  $F_{PTO}(t)$ , where this scaled PTO force is represented as,

$$u_q(t) = \frac{F_{PTO}(t)}{M + m_\mu} = -\frac{\lambda'_{fd} i_q(t) \frac{\pi}{\tau}}{M + m_\mu} = -i_q(t) \psi \quad (9)$$

where  $\lambda'_{fd} = \frac{p}{2} \lambda_{fd}$ ,  $\lambda_{fd}$  is the flux linkage,  $p$  is the number of poles and  $\tau$  is the pole pitch. This realistic PTO has associated losses, which must be taken into account when maximising the electrical power extracted from the wave, [11],

[18]. In this work a cascade control scheme is used, where an economic MPC sends piecewise linear set points to a faster inner control loop that controls the current of the LPMG to produce the desired PTO force. Field weakening is not included within the optimisation as it is assumed for simplicity that the non-linear voltage constraint is ignored.

### C. Model Predictive Control

The objective of this economic MPC is to maximise the average electrical power absorbed from the combined WEC and LPMG system, where the average power is represented as (10),

$$P_e = -\frac{1}{T} \int_{t=0}^T \left( (M + m_\mu) u_q(t) \dot{z}(t) + \frac{R}{\psi^2} u_q^2(t) \right) dt \quad (10)$$

This continuous average electrical power equation can be transformed into a discrete form using the trapezoidal rule. This discrete average electrical power approximation  $J(k)$  (11) can be maximised using quadratic programming (QP) over the prediction horizon  $N$ , to produce the optimal PTO forces over the horizon  $u_q(k+i)$ .

$$J(k) = \frac{1}{2} u_q(k+N) \dot{z}(k+N) + \sum_{i=1}^N u_q(k+i) \dot{z}(k+i) + \frac{R(M + m_\mu)}{(\lambda'_{fd} \frac{\pi}{\tau})^2} \left( \frac{1}{2} u_q^2(k+N) + \sum_{i=1}^N u_q^2(k+i) \right) \quad (11)$$

1) *Prediction model:* To implement MPC as the main outer controller, the system is discretised using a First Order Hold (FOH). The FOH produces an outer piecewise linear trajectory, which is easily tracked by a faster inner PI current controller. The discrete state space model is,

$$\mathbf{x}_f(k+1) = A_f \mathbf{x}_f(k) + B_f \Delta u_q(k+1) + F_f \Delta v(k+1) \quad (12)$$

$$\mathbf{y}_f(k) = C_f \mathbf{x}_f(k)$$

$$\mathbf{x}_f(k) = \begin{bmatrix} \mathbf{x}(k) \\ u_q(k) \\ v(k) \end{bmatrix} \quad \mathbf{y}_f(k) = \begin{bmatrix} \mathbf{y}(k) \\ u_q(k) \end{bmatrix}$$

$$A_f = \begin{bmatrix} e^{A_c T_L} & \Lambda & \Lambda \\ \mathbf{0} & 1 & 0 \\ \mathbf{0} & 0 & 1 \end{bmatrix} \in \mathbb{R}^{(n+4) \times (n+4)}$$

$$B_f = \begin{bmatrix} \Gamma \\ \Gamma \\ 0 \end{bmatrix} \quad F_f = \begin{bmatrix} \Gamma \\ 0 \\ 1 \end{bmatrix} \in \mathbb{R}^{(n+4) \times 1}$$

where  $\Lambda = A_c^{-1} (e^{A_c T_L} - I) B_c \in \mathbb{R}^{(n+2) \times 1}$ ,  $\Gamma = \frac{1}{T_L} A_c^{-1} (\Lambda - T_L B_c) \in \mathbb{R}^{(n+2) \times 1}$  and  $T_L$  is the outer sampling time.

The output vector of the system can be predicted over the prediction horizon (13), where it is assumed that the future excitation wave forces are known,

$$\hat{\mathbf{y}}_f(k) = P \mathbf{x}_f(k) + H_a \Delta \hat{\mathbf{u}}_q(k) + H_w \Delta \hat{\mathbf{v}}(k). \quad (13)$$

where

$$\hat{\mathbf{y}}_f(k) = \begin{bmatrix} y_f(k+1|k) \\ \vdots \\ y_f(k+N|k) \end{bmatrix} \quad P = \begin{bmatrix} CA \\ CA^2 \\ \vdots \\ CA^N \end{bmatrix} \quad (14)$$

where  $P \in \mathbb{R}^{3N \times (n+4)}$  and  $\hat{\mathbf{y}}_f(k) \in \mathbb{R}^{3N \times 1}$ .

$$H_a = \begin{bmatrix} CB & 0 & \dots & 0 \\ CAB & CB & \dots & 0 \\ \vdots & \vdots & \ddots & \vdots \\ CA^{N-1}B & CA^{N-2}B & \dots & CB \end{bmatrix} \in \mathbb{R}^{3N \times N} \quad (15)$$

$$H_w = \begin{bmatrix} CF & 0 & \dots & 0 \\ CAF & CF & \dots & 0 \\ \vdots & \vdots & \ddots & \vdots \\ CA^{N-1}F & CA^{N-2}F & \dots & CF \end{bmatrix} \in \mathbb{R}^{3N \times N} \quad (16)$$

The cost function (11) can then be represented in matrix form (17).

$$J(k) = \frac{1}{2} \hat{\mathbf{y}}_f(k)^T Q \hat{\mathbf{y}}_f(k) \quad (17)$$

where  $Q \in \mathbb{R}^{3N \times 3N}$  and  $M \in \mathbb{R}^{3 \times 3}$

$$Q = \begin{bmatrix} M & 0 & \dots & 0 \\ 0 & M & \dots & 0 \\ \vdots & \vdots & \ddots & \vdots \\ 0 & 0 & 0 & \frac{1}{2}M \end{bmatrix} \quad M = \begin{bmatrix} 0 & 0 & 0 \\ 0 & 0 & 1 \\ 0 & 1 & 2G \end{bmatrix}$$

and

$$G = \frac{R(M + m_\mu)}{(\lambda'_{fd} \frac{\pi}{\tau})^2},$$

yielding,

$$J = \frac{1}{2} \Delta \hat{\mathbf{u}}_q^T H_a^T Q H_a \Delta \hat{\mathbf{u}}_q + \Delta \hat{\mathbf{u}}_q^T H_a^T Q (P \mathbf{x}_f + H_w \Delta \hat{\mathbf{v}}) \quad (18)$$

The semi-positive definite cost function (18) can be solved using Quadratic Programming (QP) methods, which can be used to minimise the cost function across the prediction horizon, subject to constraints.

### III. MODEL MISMATCH

In previous work there have been positive results in absorbing maximum electrical power from a cylindrical WEC. However, typically the hydrodynamics model used in the MPC control system was the same as the system simulation model itself. For normal tracking MPC the system can track the system reference points with some robustness; however, with economic MPC the objective is to maximise the electrical power which is dependent on the systems model and cost function. With the MPC so finely tuned to maximise the average electrical power from the ideal system, this mismatch could lead to a reduction in the average electrical power

absorption. In this section the model mismatch effects between the control model and the system is investigated.

The main factors of model mismatch include: the mass of the WEC (which could increase due to future bio-fouling), the hydrostatic stiffness coefficient (which would change if there is dynamic change in cross sectional area), the radiation kernel and the non-linear viscosity effect (which could fluctuate during bio-fouling growth). For each of these factors the average electrical power absorbed is compared against a matched and a mismatched MPC system.

### A. Mass Variation

In this section the mismatch between the WEC mass in the control model and the system model is analysed. In reality the modelling mismatch of the WEC mass should be very little. However to vigorously test the control system during this mass mismatch, the control model was kept constant at the nominal plant model and the WEC model mass was varied by  $\pm 10\%$  and  $\pm 20\%$  from the nominal model. For this analysis the system was excited by 1 m high monochromatic waves and was controlled by a linearly constrained economic MPC; the effects on the average electrical absorbed power from the WEC mass mismatch is shown in Fig. 2. To have a fair analysis of the mismatch, the same systems were then tested with matching control models where the controller model has been returned to be the same as the perturbed plant. Fig. 3 shows the ratio of the average power extracted from the mismatched system to that obtained if the controller model is returned to match the perturbed plant.

From Fig. 2 it is clearly shown that when the mass of the WEC changes, there is an obvious shift in average electrical power across the monochromatic spectrum. This figure shows the effect that the change in WEC mass has on the average power. However Fig. 3 shows that the results obtained from the mismatched systems are not necessarily poor. Here it is shown that the mismatched system performs well (with a power ratio between 1 and 0.9) until the mismatched system starts to operate in frequencies higher than  $1.1 \text{ rad.s}^{-1}$ , where the average electrical powers absorbed between the mismatched and matched systems start to diverge.

### B. Hydrostatic Stiffness Coefficient Variation

The mismatch between the control model and the system model was then tested with changes in the hydrostatic stiffness. It is known from other research that non-linear effects produced from hydrodynamic Froude Krylov forces can affect the performance of the system, especially if the system is being actively controlled [19] or if the WEC has a variable cross sectional area; which in this case, it does not. With the employment of active control in this paper, it is essential that the mismatch in the hydrostatic stiffness coefficient is thoroughly tested. As before, the average electrical power absorbed from the mismatched system was compared against the average power absorbed from the fully matched model when excited by 1 m high monochromatic waves.

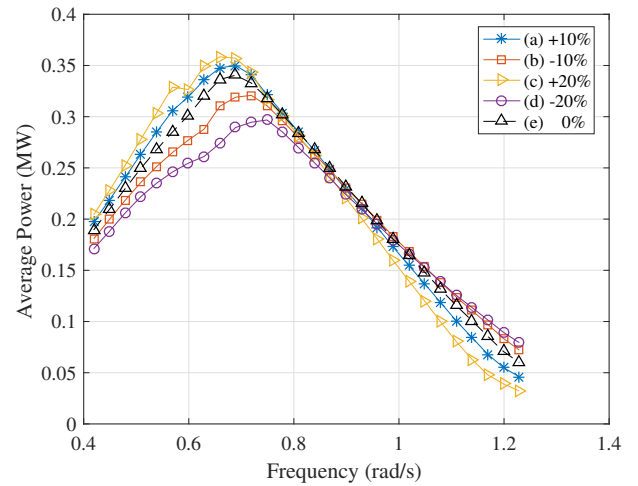


Fig. 2. Average electrical powers during a WEC mass mismatch of (a) +10%, (b) -10%, (c) +20%, (d) -20% and (e) a fully matched system

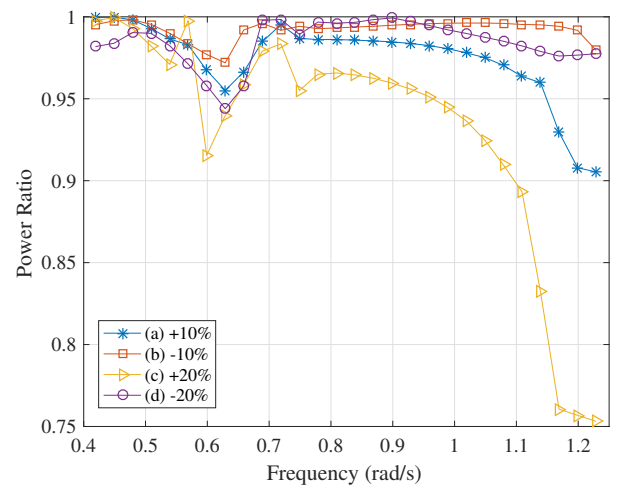


Fig. 3. Power ratio (average power from mismatched system/average power from matched system) during a WEC mass mismatch of (a) +10%, (b) -10%, (c) +20%, (d) -20%

The average electrical power absorbed from the mismatched models are shown in Fig. 4, while the ratio of the average power absorbed from the mismatch to the matched systems (with controller model returned to match the perturbed system) are shown in Fig. 5.

As seen in Fig. 4, when there are mismatches between the system model and the control model, there are minor average power differences after  $0.9 \text{ rad.s}^{-1}$ . However, there are substantial average power differences over lower frequencies (i.e.  $0.1 \times 10^6 \text{ W}$  between systems with a 0% and +20% mismatch at  $0.7 \text{ rad.s}^{-1}$ ). Therefore the extracted average electrical power from the system is highly dependent on the change in the hydrostatic stiffness coefficient. Even though the average power significantly fluctuates depending on the hydrostatic stiffness, the mismatch between the control model and the system model seems to have hardly any effect on the amount of average electrical power absorbed from the mismatched system, as can be seen in Fig. 5. The worst case

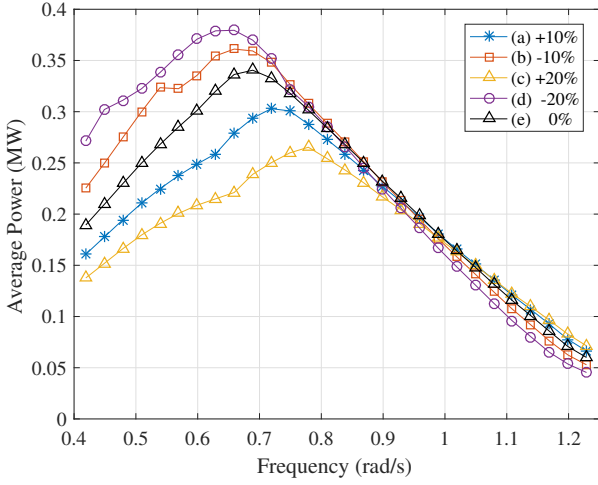


Fig. 4. Average electrical powers during a hydrostatic stiffness coefficient mismatch of (a) +10%, (b) -10%, (c) +20%, (d) -20% and (e) a fully matched system

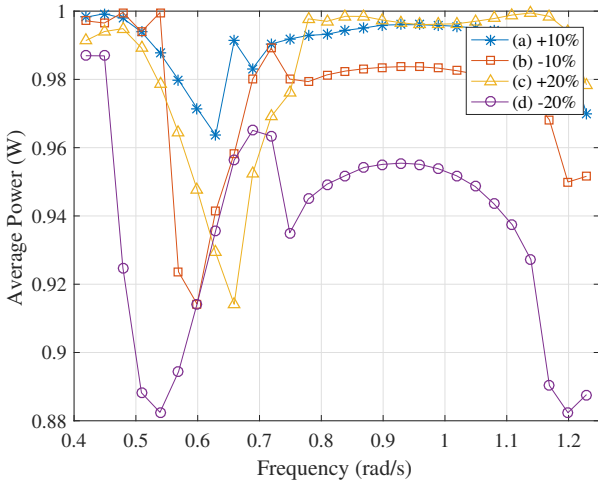


Fig. 5. Power ratio (average power from mismatched system/average power from matched system) during a hydrostatic stiffness coefficient mismatch of (a) +10%, (b) -10%, (c) +20%, (d) -20%

was during the  $-20\%$  model mismatch where the the power ratio dropped to 0.88. Furthermore, the use of an MPC with a hydrostatic stiffness mismatch in the control model can still produce an acceptable amount of average electrical power.

### C. Radiation Kernel Variation

This subsection focusses on the mismatch between the control model and the system model in terms of uncertainty in the radiation kernel. The mismatched system was tested as before where the mismatched system was excited with 1 m high monochromatic waves. The system mismatch was achieved by varying the gain, poles and zeros of the radiation kernel within the mismatch percentages of 10% and 20%. To test this mismatch in an unbiased manner, multiple variations of the mismatched radiation kernels had to be analysed since the radiation kernel is dependent on a number of parameters. The amount of tested randomised radiation kernel systems was increased until the mean average electrical power values

equalled the average power absorbed from an ideal matched system.

Fig. 6 shows the monte-carlo results for the average electrical power absorbed from the system with a radiation kernel mismatch percentage of  $\pm 10\%$  and  $\pm 20\%$ . For example at  $0.7 \text{ rad.s}^{-1}$ , the range of power extracted is anywhere between 0.28 and 0.36 MW, for combinations of the kernel parameters (gains, zeros and poles) perturbed in the range  $\pm 20\%$  about their nominal values.

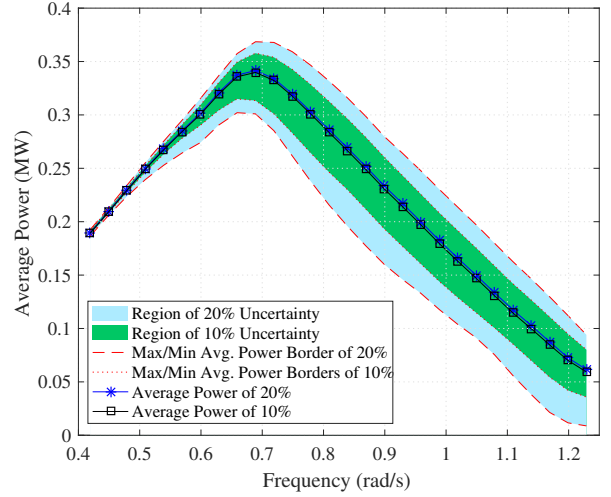


Fig. 6. Average electrical power for a) matched, b)  $\pm 10\%$  and c)  $\pm 20\%$  mismatch. The  $\pm 10\%$  and  $\pm 20\%$  boundaries are also shown.

The change in radiation kernel has a great effect on the absorbable average electrical power, as shown in Fig. 6. To have a fair comparison, the power extracted for the mismatched radiation kernel systems that caused the maximum and minimum average power points for both  $\pm 10\%$  and  $\pm 20\%$  are now compared to the performance of the matched control systems. Fig. 7 shows the power ratio, comparing the average power extracted when the system radiation kernel is mismatched to the controller, to the average electrical power extracted when the controller model is retuned to match the system. It is shown that over low frequencies of  $(0.4 - 1.05) \text{ rad.s}^{-1}$  that the mismatched control model produce acceptable results since the power ratio is higher than 0.9 for both  $\pm 10\%$  and  $\pm 20\%$  cases. However for frequencies  $> 1 \text{ rad.s}^{-1}$ , the power ratios for the mismatched system begin to degrade. The worst case is when the minimum power for a 20% mismatch in the radiation kernel during high frequencies, leading to a power ratio of 0.25. This may seem unacceptable, however depending on the spectrum of the excitation waves, the power content at those frequencies may actually be inconsequential.

### D. Non-Linear Viscosity Variation due to Biofouling

The non-linear viscosity force  $F_v(t)$ , is based on the semi-empirical Morison equation [20],

$$F_v(t) = -C_{vis}(t) (\dot{z}(t) - \dot{\eta}(t)) \quad (19)$$

where,

$$C_{vis}(t) = \frac{1}{2} \rho C_d A |\dot{z}(t) - \dot{\eta}(t)|.$$



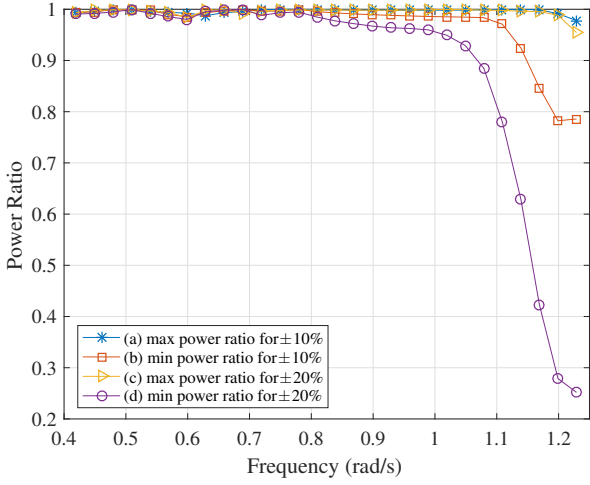


Fig. 7. Power ratio (average power from mismatched system/average power from matched system) during a radiation kernel mismatch of (a) max power ratio for  $\pm 10\%$ , (b) min power ratio for  $\pm 10\%$ , (c) max power ratio for  $\pm 20\%$ , (d) min power ratio for  $\pm 20\%$

Here  $\rho$  is the density of water,  $C_d$  is the drag coefficient [21] and  $A$  is the cross sectional area of the point absorber. In recent research there has been a focus on the non-linear effects that viscosity has on the performance of the system [22]. The non-linear contribution of viscosity is shown in the system model (20),

$$\frac{d}{dt} \begin{bmatrix} z(t) \\ \dot{z}(t) \\ \mathbf{x}_r(t) \end{bmatrix} = A_c(t) \begin{bmatrix} z(t) \\ \dot{z}(t) \\ \mathbf{x}_r(t) \end{bmatrix} + B_c u_q(t) + F_c v(t) + E_c(t) \dot{\eta}(t) \quad (20)$$

where,

$$A_c(t) = \begin{bmatrix} 0 & 1 & \mathbf{0} \\ -\frac{\beta}{M+m_\mu} & -\frac{(D_r+C_{vis}(t))}{M+m_\mu} & -\frac{C_r}{M+m_\mu} \\ 0 & B_r & A_r \end{bmatrix}$$

$$F_c = B_c = \begin{bmatrix} 0 \\ 1 \\ \mathbf{0} \end{bmatrix} \quad E_c(t) = \begin{bmatrix} 0 \\ \frac{C_{vis}(t)}{M+m_\mu} \\ \mathbf{0} \end{bmatrix} \quad \mathbf{x}(t) = \begin{bmatrix} z(t) \\ \dot{z}(t) \\ \mathbf{x}_r(t) \end{bmatrix} \quad (21)$$

Variations in the viscosity force could be caused by increasing growth of biofouling on the WEC itself, which could change the hydrodynamic properties of the WEC. Furthermore, it is important to analyse the effects that the mismatched control model has on the average power absorbed from the viscous system, since the viscous drag coefficient could vary around a certain value in practice. In [22] it was shown that with the inclusion of the non-linear viscosity term in the hydrodynamics, that the average power production was drastically reduced. A non-linear economic MPC was implemented which showed that the average power could still be maximised even with viscosity included. A linear MPC was then implemented which showed promising results that concluded that a constant linear viscosity approximation used in a linear MPC could produce similar results to a computational expensive non-linear MPC.

In this work, the non-linear viscosity drag coefficient is inserted into the hydrodynamic system excited again by 1 m high monochromatic excitation waves. The economic MPC with a linear viscous approximation, as shown in [22], is used in this work. Fig. 8 shows the resulting absorbed average electrical power found from  $\pm 10\%$  and  $\pm 20\%$  mismatched viscous coefficient. Here there is a small variation in the absorbed average power. Fig. 9 shows the power ratio that the matched system has against the mismatched system. In this case the matched system used the non-linear MPC from [22], to produce the best possible results for the matched system. It is shown in Fig. 9 that the power ratios for both the  $\pm 10\%$  and  $\pm 20\%$  cases are all above 0.91; therefore the linear viscous approximated MPC is acceptable for use when the viscosity is uncertain.

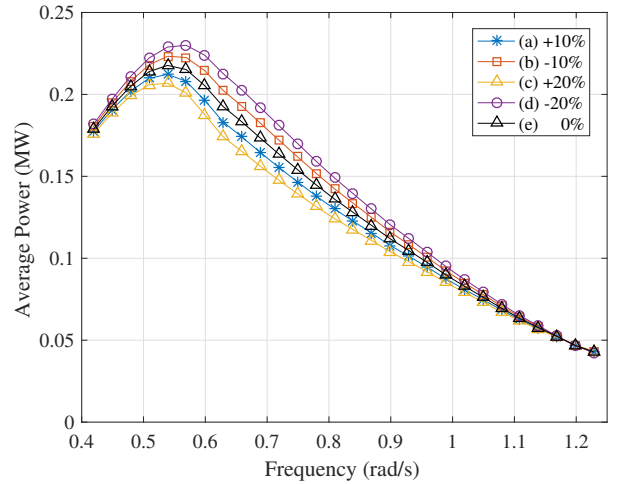


Fig. 8. Average electrical powers during a non-linear drag coefficient mismatch of (a) +10%, (b) -10%, (c) +20%, (d) -20% and (e) a fully matched system

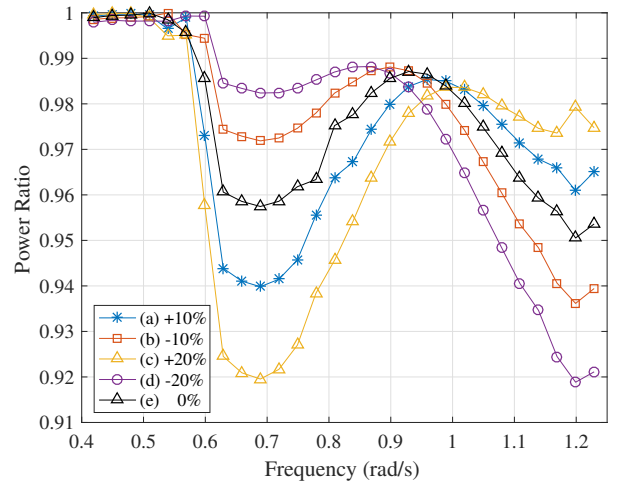


Fig. 9. Power ratio (average power from mismatched system using linearly estimated MPC/average power from matched system using a non-linear MPC) during a non-linear drag coefficient mismatch of (a) +10%, (b) -10%, (c) +20%, (d) -20% and (e) a fully matched system

#### IV. MOVE-BLOCKING CONTROL HORIZON

Economic MPC controller typically uses a control horizon of  $N_c < N$  free control choices over the prediction horizon. The computational burden can be lowered by decreasing  $N_c$ , but at the cost of reducing performance.

As shown in section. III, all the system mismatches between the control model and system model can affect the amount of absorbable average electrical power. In this section, the effects of a reduced control horizon  $N_c$  on the mismatched systems performance is investigated. Two types of control horizons are used in this paper. First a standard control horizon reduction is applied where the control variables  $\Delta u_q(k+i)$  are set to zero after the first  $N_c$  steps of the prediction horizon,

$$\Delta \mathbf{u}_{qh}(k) = \begin{bmatrix} \mathbf{I}_{N_c} & \mathbf{0}_{N_c \times N_r} \\ \mathbf{0}_{N_r \times N_c} & \mathbf{0}_{N_r \times N_r} \end{bmatrix} \Delta \mathbf{u}_q(k),$$

where  $N_r = (N - N_c)$ .

The second being a move-blocking technique where the  $N_c$  control variables are appropriately spread out across the prediction horizon  $N$ , with the control variables concentrated over the early stages of the prediction horizon,

$$\Delta \mathbf{u}_{qm}(k) = \begin{bmatrix} \Phi_1 & \mathbf{0} & \dots & \mathbf{0} \\ \mathbf{0} & \Phi_2 & \dots & \mathbf{0} \\ \vdots & \vdots & \ddots & \vdots \\ \mathbf{0} & \mathbf{0} & \dots & \Phi_{N_c} \end{bmatrix} \Delta \mathbf{u}_q(k)$$

where,

$$\Phi_j = [ \mathbf{1}_{n_j \times 1} \quad \mathbf{0}_{n_j \times (n_j - 1)} ] \in \mathbb{R}^{n_j \times n_j},$$

where matrix  $\mathbf{n} \in \mathbb{R}^{N_c \times 1}$  and  $\sum_{j=1}^{N_c} n_j = N$ .

It is clearly shown from the waveforms in Fig. 10 that as the control horizon  $N_c$  decreases, the control action across the prediction horizon becomes more disjoint and diverges from the control waveform when  $N_c = N$ ; this results in the deterioration of average power. However, by incorporating a move-blocking system in the control horizon, less control variables need to be calculated. Therefore, there needs to be a balance between minimising the amount of control variables and maintaining an acceptable amount of absorbed average power.

##### A. Move-Blocking Control Horizon Performance

First, the performance of the MPC with a perfect (matched) hydrodynamic model was investigated using a full control horizon, a reduced control horizon and a move-blocking control horizon. For all tests, a 1 m monochromatic excitation wave was used; linear constraints were assumed for WEC heave and velocity and for the PTO force. Fig. 11 shows the average electrical powers absorbed from the system when the different types of control horizons were used. When a standard reduced horizon is used with  $N_c = 30$ , the average power has drastically diminished when compared to the average power results found when using a full control horizon with  $N_c = N$ .

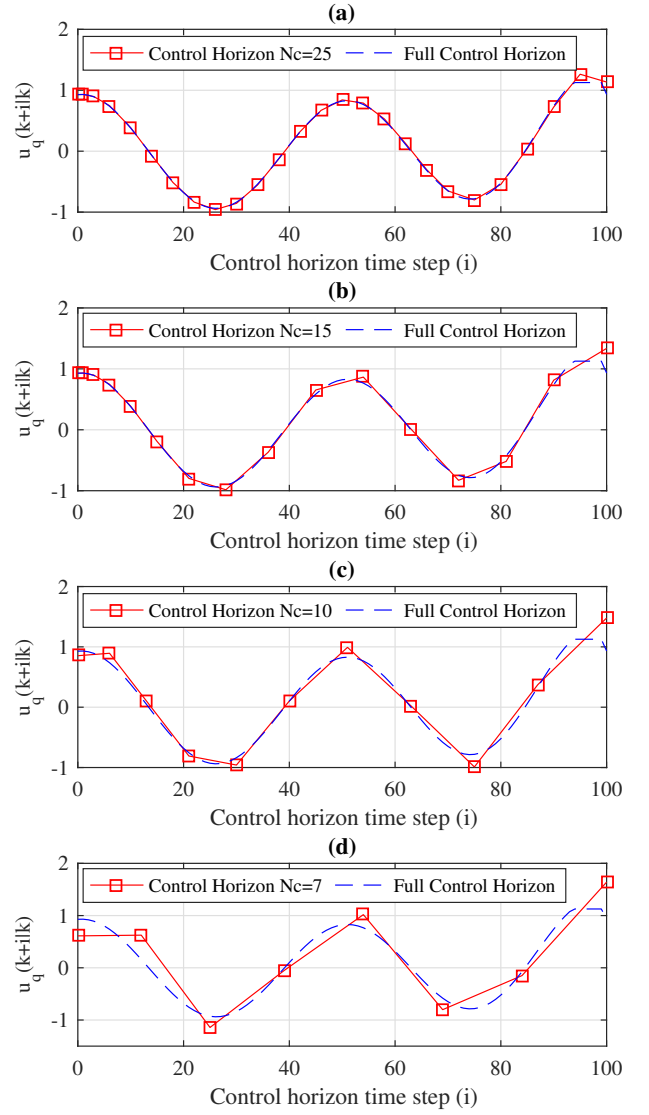


Fig. 10. A comparison between the control variables  $u_q(k+i)$  created when using a full control horizon ( $N_c = 100$ ) and when a move-blocking control horizon of (a)  $N_c = 25$ , (b)  $N_c = 15$ , (c)  $N_c = 10$  and (d)  $N_c = 7$  is used

However, when a move-blocking control horizon of  $N_c = 10$  was used, the average power extracted was observed to be very close to that obtained with a full control horizon of  $N_c = N = 100$ . However, any decrease from  $N_c = 10$  with the moving-block technique resulted in a degradation of the average power. Nevertheless, the average power results from the move-blocking technique for  $N_c < 10$  show much improved power levels when compared with the standard control horizon reduction with a much greater control horizon  $N_c$ .

To show the serious advantages of using a move-blocking control horizon, the average optimisation solution times for the unconstrained and linearly constrained problems were recorded. As shown in Fig. 12, the difference between the solution times for constrained and unconstrained MPC is very clear. However, for both unconstrained and constrained cases



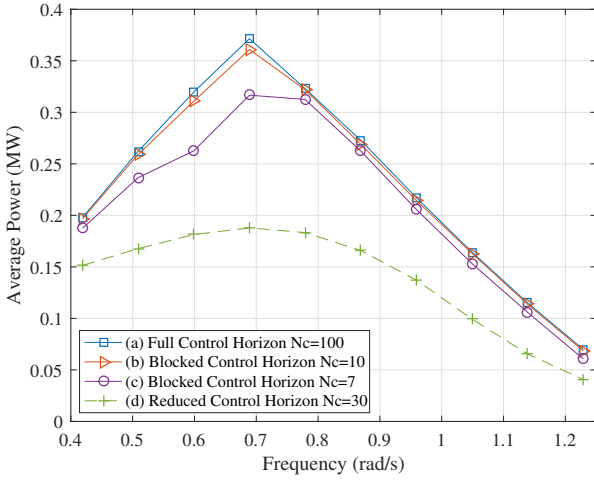


Fig. 11. Average electrical power absorbed when (a) a full control horizon is used, (b) a move-blocked control horizon of  $N_c = 10$  is used, (c) a move-blocked control horizon of  $N_c = 7$  is used and (d) a reduced control horizon of  $N_c = 30$  is used

the solve time decreases as the control horizon  $N_c$  decreases, with the constrained optimisation solution time decreasing at a much higher rate than the unconstrained optimisation. Furthermore, this figure also shows the corresponding power ratio obtained for the various control horizons. The power ratio here is the ratio of the average power extracted using a reduced move-blocking horizon against the average power extracted when a full control horizon is used. It is clearly shown that as the control horizon  $N_c$  is reduced, the power ratio stays at unity until the control horizon  $N_c < 15$ , when the power ratio begins to decrease. From this figure, it is shown that the optimisation of the problem can be simplified without diminishing the performance of the average power extraction from the system.

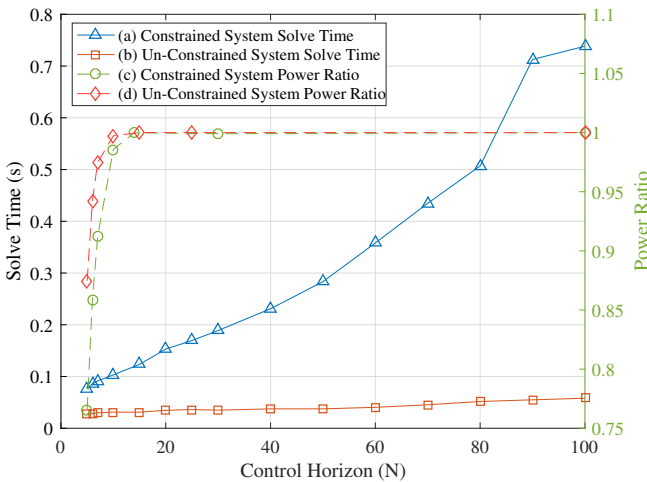


Fig. 12. (Left axis) The optimisation solve time vs the control horizon  $N_c$  (a) with constraints, (b) without constraints; (Right axis) The power ratio (average power from an MPC with control horizon  $N_c$ /average power from an MPC with a full control horizon) vs the control horizon  $N_c$  (a) with constraints (b) without constraints

## B. System Robustness during system mismatch

Here the move-blocking technique, as shown in section. IV, is used on a mismatched system where the robustness of the system will be analysed. From section. III it was shown that some mismatches within the system can affect the average power extracted from the system, with some characteristics having more of an effect on the outcome than others. Here the hydrostatic mismatch (section III-B) in the system is used in the robustness analysis since it affects the average power extraction the most at lower frequencies, where the system will spend the majority of its operating time.

To test the robustness of the system, the move-blocking technique was used on the mismatched hydrostatic system where a  $-20\%$  hydrostatic stiffness coefficient was used; 1 m high monochromatic waves are used in this analysis. The resulting extracted average electrical power from the mismatched system are shown in Fig. 13. From Fig. 13 it is shown that to some degree, the inclusion of the move-blocking technique does not cause any significant difference in performance. It is only when the control horizon has been decreased to the point ( $N_c = 10$ ) where  $\Delta u_q(k+2)$  is forced to become the same as  $\Delta u_q(k+1)$  that the average power starts to significantly deviate from the average power extracted when using a full control horizon.

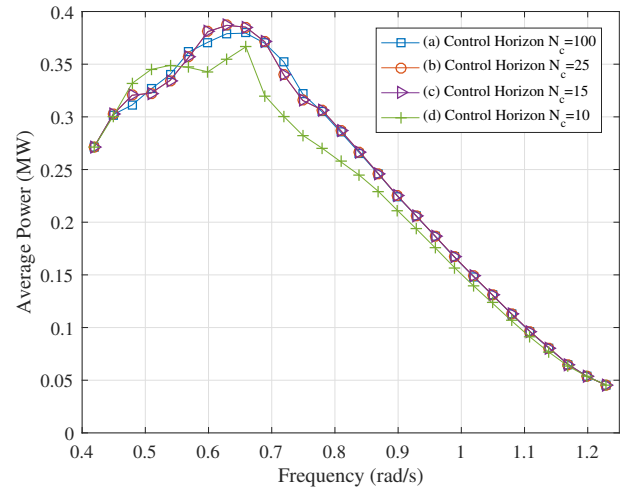


Fig. 13. Average electrical powers during a hydrostatic stiffness mismatch of  $-20\%$  when a control horizon of (a)  $N_c = 100$  (full control horizon), (b)  $N_c = 25$ , (c)  $N_c = 15$  and (d)  $N_c = 10$

On the other hand, when move-blocking results in a  $\Delta u_q(k+2)$  and  $\Delta u_q(k+1)$  which are equal to each other, the calculated PTO force  $\Delta u_q(k)$  becomes damped; this is shown in Fig. 14. This damped PTO force control action can lead to problems in satisfying the hard constraints.

In Fig. 15 it is shown for a 1 m high monochromatic wave with a frequency of  $0.419 \text{ rad.s}^{-1}$  that the heave of the WEC and LPMG stay within the heave limitation of  $\pm 3.5 \text{ m}$  when a control horizon of  $N_c = 100$  is used. However, when a control horizon of  $N_c = 10$  is implemented, the PTO force (Fig. 14) becomes more damped and the heave of the system starts to exceed the heave limitation, which

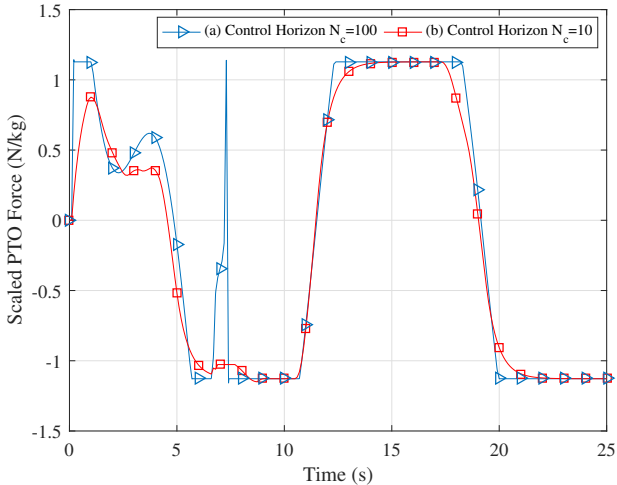


Fig. 14. The scaled PTO force  $u_q(t)$  during a 1 m,  $0.4487 \text{ rad.s}^{-1}$  monochromatic excitation wave when an MPC with a control horizon of (a)  $N_c = 100$  (full control horizon) and (b)  $N_c = 10$  are used

could cause damage. If the control horizon  $N_c$  is too low, then there is a higher chance of  $\Delta u_q(k+2) = \Delta u_q(k+1)$  which would degrade the systems performance. However, as stated in section. IV-A, if the control horizon  $N_c$  is selected too high, then the optimisation solve time will increase. Therefore, there needs to be a compromise where the move-blocking control horizon is wisely chosen to have the lowest possible control horizon whilst having acceptable system performance which obeys the systems constraints.

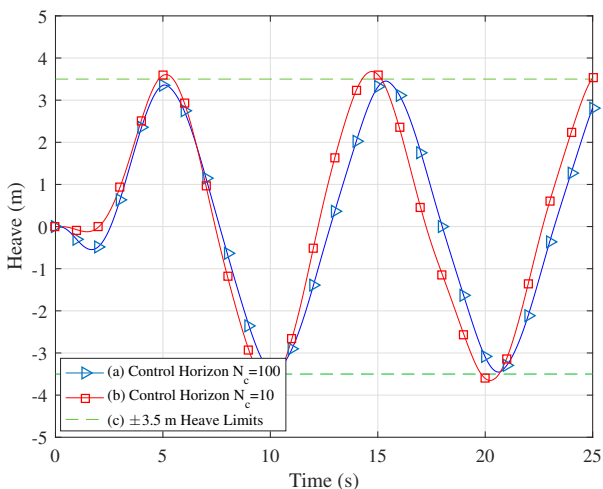


Fig. 15. The WEC heave  $z(t)$  during a 1 m,  $0.6613 \text{ rad.s}^{-1}$  monochromatic excitation wave when an MPC with a control horizon of (a)  $N_c = 100$  (full control horizon) and (b)  $N_c = 10$  are used

## V. CONCLUSION

In section. III, each characteristic in the hydrodynamic model was analysed with a degree of model mismatch introduced between the control system and the actual system. System model characteristics such as, WEC mass, hydrostatic coefficient, the radiation kernel and the coefficient  $C_d$  of the non-linear viscosity were varied by up to  $\pm 20\%$  from

the control model. The results showed that each mismatch introduced a certain degree of average electrical power loss when it was compared to the average electrical power absorbed from a fully matched system. Sections. III-A and III-C showed the effects that the mismatches had on the average electrical power. These two section showed similar results where the difference in average power between the mismatched and fully matched systems was acceptable up to  $1 \text{ rad.s}^{-1}$ . For frequencies  $\omega > 1 \text{ rad.s}^{-1}$  the average power between the matched and mismatched systems started to diverge. From a mathematical point of view, this seems unacceptable. However, from a practical point of view the fundamental frequency of a realistic excitation wave spectrum would be much lower, therefore the effects from the higher frequencies would seem negligible. The mismatch effects shown in section. III-D are nearly inconsequential, considering that the power ratio between the matched and mismatched systems was no worse than 0.92. Section. III-B showed that at lower frequencies (frequencies that would actually be active during a realistic sea spectrum), there were large changes in average electrical power when the hydrostatic coefficient varied between  $\pm 20\%$  (eg. at  $0.65 \text{ rad.s}^{-1}$  there was 0.155 MW of a difference in average power between the systems with a  $\pm 20\%$  hydrostatic coefficient mismatch). Even though the smallest power ratio produced from the hydrostatic coefficient mismatch was 0.88, this power ratio drop occurred during the lower frequencies where there would be a much greater effect due to the system's inherent sensitivity to hydrostatic coefficient changes.

In section. IV, a move-blocking technique was incorporated into the control horizon. The move-blocking method allowed for a reduction of the number of free control variables needed to be calculated. Unlike other control horizon minimisation techniques where a reference trajectory is used, the move-blocking technique is better suited to this economic MPC application due to its ability to represent the pseudo periodic nature of the control action across the prediction horizon with a small number of free control variables. It was shown in section. IV-A that this economic MPC can still produce an exceptional amount of power even with a reduced control horizon of  $N_c = 10$  whilst reducing the optimisation computation time by 87%.

In section. IV-B, the move-blocking technique was then tested on a mismatched system, with a  $-20\%$  mismatched hydrostatic coefficient. It was shown that the inclusion of move-blocking in the control horizon had a minor affect on the absorption of average electrical power when compared to a full control horizon. However, it was clear that if the control horizon was set low enough yielding  $\Delta u_q(k+1) = \Delta u_q(k+2)$  then the control action would dampen, which then causes the system to exceed the systems constraints which may lead to damage. Therefore, using a move-block technique for the control horizon whilst operating in a mismatched system is highly advantageous once the allocation of the control variables within the control horizon are arranged in a manner that there is enough resolution at the beginning of the prediction horizon.

## ACKNOWLEDGEMENT

This work was supported through the Science Foundation Ireland research centres program, (SFI 12/RC/2302).

## REFERENCES

- [1] B. Drew, A. R. Plummer, and M. N. Sahinkaya, "A review of wave energy converter technology," *Proceedings of the Institution of Mechanical Engineers, Part A: Journal of Power and Energy*, vol. 223, no. 8, pp. 887–902, 2009.
- [2] K. Budal and J. Falnes, "A resonant point absorber of ocean-wave power," *Nature*, vol. 256, p. 478, 1975.
- [3] —, "Interacting point absorbers with controlled motion," in *Power from Sea Waves*, 1980, pp. 381–399.
- [4] —, "Optimum operation of improved wave-power converter," *Marine Science Communications*, vol. 3, pp. 133–150, 1977.
- [5] a. Babarit, G. Duclos, and a.H. Clément, "Comparison of latching control strategies for a heaving wave energy device in random sea," *Applied Ocean Research*, vol. 26, no. 5, pp. 227–238, jul 2004.
- [6] F. Fusco and J. Ringwood, "Suboptimal Causal Reactive Control of Wave Energy Converters Using a Second Order System Model WEC," *Proceedings of the 21st International Offshore and Polar Engineering Conference*, pp. 1–8, 2011.
- [7] E. Abraham and E. Kerrigan, "Optimal active control and optimization of a wave energy converter," ... *Energy, IEEE Transactions on*, vol. 4, no. 2, pp. 1–8, 2013.
- [8] R. Genest and J. V. Ringwood, "Receding Horizon Pseudospectral Control for Energy Maximization With Application to Wave Energy Devices," *IEEE Transactions on Control Systems Technology*, vol. 25, no. 1, pp. 29–38, 2016.
- [9] J. M. Maciejowski, *Predictive Control: with Constraints*, ser. Pearson Education. Prentice Hall, 2002.
- [10] J. Cretel, G. Lightbody, G. P. Thomas, and A. W. Lewis, "Maximisation of energy capture by a wave-energy point absorber using model predictive control," in *IFAC Proceedings Volumes (IFAC-PapersOnline)*, vol. 18, no. PART 1, 2011, pp. 3714–3721.
- [11] A. C. O'Sullivan and G. Lightbody, "Wave to Wire Power Maximisation from a Wave Energy Converter," in *In Proceedings of the 11th European Wave and Tidal Energy Conference (EWTEC)*, Nantes, 2015.
- [12] —, "Co-design of a wave energy converter using constrained predictive control," *Renewable Energy*, vol. 102, pp. 142–156, mar 2017.
- [13] C. Wright, J. Murphy, C. S. W. V. Pakrashi, and J. Murphy, "The Dynamic Effects of Marine Growth on a Point Absorbing Wave Energy," in *Offshore Energy & Storage Symposium and Industry Connector*, no. July, 2016.
- [14] R. Genest and J. V. Ringwood, "A critical comparison of model-predictive and pseudospectral control for wave energy devices," *Journal of Ocean Engineering and Marine Energy*, vol. 2, no. 4, pp. 1–15, 2016.
- [15] R. Cagienard, P. Grieder, E. C. Kerrigan, and M. Morari, "Move blocking strategies in receding horizon control," *Journal of Process Control*, vol. 17, no. 6, pp. 563–570, 2007.
- [16] W. E. Cummins, "The Impulse Response Function and Ship Motions," *Schiffstechnik*, vol. 9, pp. 101–109, 1962.
- [17] C.-H. Lee, *WAMIT Theory Manual*, 1995.
- [18] A. C. M. O'Sullivan and G. Lightbody, "Predictive control of a wave to wire energy conversion system - the importance of field weakening," in *2016 UKACC 11th International Conference on Control (CONTROL)*, no. August, 2016, pp. 1–6.
- [19] G. Giorgi, M. Pe, and J. V. Ringwood, "Nonlinear Hydrodynamic Models for Heaving Buoy Wave Energy Converters," 2016.
- [20] J. R. Morison, J. W. Johnson, S. A. Schaaf, and Others, "The force exerted by surface waves on piles," *Journal of Petroleum Technology*, vol. 2, no. 05, pp. 149–154, 1950.
- [21] M. Bhinder, A. Babarit, L. Gentaz, and P. Ferrant, "Assessment of viscous damping via 3d-cfd modelling of a floating wave energy device," in *9th European Wave and Tidal Energy Conference*, 2011.
- [22] A. C. M. O'Sullivan and G. Lightbody, "The Effect of Viscosity on the Maximisation of Electrical Power from a Wave Energy Converter under Predictive Control," in *The 20th World Congress of the International Federation of Automatic Control*, 2017.